THE JOURNAL OF BIOLOGICAL CHEMISTRY
Vol. 275, No. 13, Issue of March 31, pp. 9468–9475, 2000

Printed in U.S.A.

Dimerization of *Escherichia coli* DNA-gyrase B Provides a Structural Mechanism for Activating the ATPase Catalytic Center*

(Received for publication, October 28, 1999, and in revised form, December 29, 1999)

Laurent Brino‡§, Alexandre Urzhumtsev¶, Marc Mousli‡‖, Christian Bronner‡‖, André Mitschler‡, Pierre Oudet‡, and Dino Moras‡**

From the ‡Institut de Génétique et de Biologie Moléculaire et Cellulaire (IGBMC), CNRS/INSERM, Université Louis Pasteur, BP 163, 1 Rue Laurent Fries, 67404 Illkirch Cedex, the ¶Laboratoire de Cristallographie et Modélisation des Matériaux Minéraux et Biologiques, Faculté des Sciences, Université H. Poincaré, Nancy I, BP 239, 54506 Vandœuvre-les-Nancy Cedex, and ‖INSERM U425, Faculté de Pharmacie, BP 24, 67401 Illkirch Cedex, France

DNA-gyrase exhibits an unusual ATP-binding site that is formed as a result of gyrase B subunit dimerization, a structural transition that is also essential for DNA capture during the topoisomerization cycle. Previous structural studies on *Escherichia coli* DNA-gyrase B revealed that dimerization is the result of a polypeptidic exchange involving the N-terminal 14 amino acids. To provide experimental data that dimerization is critical for ATPase activity and enzyme turnover, we generated mutants with reduced dimerization by mutating the two most conserved residues of the GyrB N-terminal arm (Tyr-5 and Ile-10 residues). Our data demonstrate that the hydrophobic Ile-10 residue plays an important role in enzyme dimerization and the nucleotide-protein contact mediated by Tyr-5 side chain residue helps the dimerization process. Analysis of ATPase activities of mutant proteins provides evidence that dimerization enhances the ATP-hydrolysis turnover. The structure of the Y5S mutant of the N-terminal 43-kDa fragment of *E. coli* DNA GyrB subunit indicates that Tyr-5 residue provides a scaffold for the ATP-hydrolysis center. We describe a channel formed at the dimer interface that provides a structural mechanism to allow reactive water molecules to access the γ-phosphate group of the bound ATP molecule. Together, these results demonstrate that dimerization strongly contributes to the folding and stability of the catalytic site for ATP hydrolysis. A role for the essential Mg^{2+} ion for the orientation of the phosphate groups of the bound nucleotide inside the reactive pocket was also uncovered by superposition of the 5′-adenylyl β-γ-imidodiphosphate (ADPNP) wild-type structure to the salt-free ADPNP structure.

DNA-gyrase (EC 5.99.1.3) is a bacterial type II topoisomerase that negatively supercoils plasmid DNA molecules *in vitro*. It is also involved in catenation and decatenation, knotting and unknotting reactions of circle DNA molecules. All these processes require the binding and the hydrolysis of ATP (1, 2). DNA-gyrase is involved in DNA replication, repair, recombination, and transcription (3).

Escherichia coli DNA-gyrase is composed of two subunits, GyrA and GyrB of 97 and 90 kDa, respectively. They associate to form an A_2B_2-active holoenzyme (4, 5). The GyrB subunit possesses two domains, a 43-kDa N-terminal domain (aa[1] 2–393) that contains the ATPase catalytic site and a 47-kDa C-terminal domain (aa 394–804) that is required for the interaction with GyrA. Kinetic studies of the ATPase activity of the GyrB subunit have provided a model in which the binding of ATP induces dimerization of the 43-kDa ATP-binding domain and activation of the catalytic center of hydrolysis (6). Dimerization is a reversible process coupled to the binding and hydrolysis of ATP bound at the dimer interface. X-ray crystallographic studies have provided the structure of the dimer of 43-kDa GyrB fragments complexed with ADPNP. The amino acids directly implicated in the nucleotide-binding site are mainly located in the N-terminal crystallographic subdomain (aa 2–220). The Tyr-5 residue, from the N-terminal extension (aa 2–16) of the second subunit that forms the dimer, partakes in a hydrogen bond to 2′-hydroxyl ribose of the bound ATP (7).

Based on biochemical and structural data of eukaryotic and prokaryotic enzymes, a catalytic clamp model for the ATP-dependent mechanism of DNA transfer into the enzyme has been proposed for type II DNA topoisomerases (8–11). In this model, the binding of ATP promotes dimerization and thus closure of the GyrB N-terminal side of A_2B_2 tetramer. This structural transition allows entry and capture of a double-stranded DNA molecule (T-DNA). The GyrA subunit catalyzes the reversible formation of a covalent linkage between its Tyr-122 residue and 5′P of another DNA duplex wrapped around the holoenzyme (~120 base pairs), called G-DNA. This results in the formation of a transient DNA gate through which the T-DNA passes. Following transport, DNA strand breaks are resealed, and the T-DNA molecule is released from the holoenzyme.

The mechanism by which ATP binding, hydrolysis, and product release are coupled to the various steps in the transport of one DNA double helix through another is of key importance in understanding reactions catalyzed by type II DNA topoisomerases. Pairing between the two N-terminal GyrB domains in the presence of ADPNP or ATP was assumed to be responsible for the conversion of an open clamp into a closed clamp protein conformation that captures a DNA molecule and is able to transfer it across the holoenzyme structure. The protein clamp opens for the next reaction when bound ATP is hydrolyzed, but if ATP is replaced by ADPNP, only a single round of DNA

* This work was supported in part by grants from Hoechst Marion Roussel, INSERM, CNRS, the Center Hospitalier Universitaire Régional, the Association pour la Recherche sur le Cancer, and the Fondation pour la Recherche Médicale. The costs of publication of this article were defrayed in part by the payment of page charges. This article must therefore be hereby marked "*advertisement*" in accordance with 18 U.S.C. Section 1734 solely to indicate this fact.

The atomic coordinates and structure factors (code 1EI1) have been deposited in the Protein Data Bank, Research Collaboratory for Structural Bioinformatics, Rutgers University, New Brunswick, NJ (http://www.rcsb.org/).

§ Supported by a fellowship from Hoechst Marion Roussel and the Association pour la Recherche sur le Cancer.

** To whom correspondence should be addressed. Tel.: 33-3-88-65-32-20; Fax: 33-3-88-65-32-76; E-mail: moras@igbmc.u-strasbg.fr.

[1] The abbreviations used are: aa, amino acids; ADPNP, 5′-adenylyl β-γ-imidodiphosphate; WT, wild-type; GST, glutathione *S*-transferase.

strand passage would occur and the enzyme would be trapped in a frozen conformation (10–12). Thus, ATP hydrolysis is considered to be required only for enzyme recycling before a next catalytic round.

A key untested prediction of the current models for gyrase function is that dimerization is critical for ATPase activity. To provide experimental evidence, we generated mutants with reduced dimerization by mutating the two most conserved residues of the GyrB N-terminal arm, Tyr-5 and Ile-10. Our data demonstrate that Ile-10 plays an important role in enzyme dimerization, and the nucleotide-protein contact mediated by Tyr-5 side chain residue is essential for helping the dimerization process. Analysis of ATPase activity show that dimerization enhances the turnover for hydrolyzing bound ATP. Our crystallographic study describes the mechanism of dimerization and the ATPase function of this enzyme.

EXPERIMENTAL PROCEDURES

Materials—The following reagents were purchased: ATP, ADPNP, and novobiocin, Sigma; epoxy-activated Sepharose, pGEX4T-3, glutathione-Sepharose resin, reduced glutathione, bovine thrombin, Amersham Pharmacia Biotech; Deep Vent DNA polymerase, New England Biolabs (Ivry-Sur-Seyne, France); isopropyl-1-thio-β-D-galactopyranoside, Euromedex (Strasbourg, France); pefabloc, Roche Molecular Biochemicals; radiolabeled nucleotides, ICN (Orsay, France). Protein concentrations were determined by the Bio-Rad protein assay using bovine serum albumin as standard.

Protein Expression and in Vitro Studies—The DNA encoding sequences of wild-type (aa 2–393) and Δ1–14 (aa 15–393, K21R) 43-kDa GyrB N-terminal fragments were amplified by PCR and subcloned into pGEX4T-3 vector for expression of the glutathione *S*-transferase (GST) fusion proteins in *E. coli*. Site-directed mutagenesis (Y5S, Y5F, and I10G) was carried out as described previously (13). GST fusion proteins were purified according to the manufacturer's instructions.

For crystallization assays, the Y5S mutant 43-kDa fragment was expressed in *E. coli* transformed with pN43-Y5S (13). Protein was purified by using a novobiocin-Sepharose column as described by Staudenbauer and Orr (14); the 5 M urea-eluted fractions containing the denatured proteins were desalted onto a Sephadex G-25 medium column equilibrated in 20 mM Tris-HCl, pH 7.5, 5 mM DTT, 1 mM EDTA. The fractions were concentrated by ultrafiltration on Amicon centricon 30 (YM-10 membrane) to 20 mg/ml.

Analysis of protein interactions of the 43-kDa fragment of the GyrB subunit was performed using the GST pull-down assay (15). The GST 43-kDa fusion protein (5 μM) was incubated with thrombin-cleaved 43-kDa fragment (40 μM) in the presence or absence of ADPNP (0.5 mM) for various times at 25 °C in 35 mM Tris-HCl, pH 7.3, 24 mM KCl, 6 mM $MgCl_2$, 5 mM DTT, 0.36 mg/ml bovine serum albumin, 6.5% glycerol supplemented (binding buffer) with 0.75 mM pefabloc (final volume of 25 μl). Glutathione-Sepharose beads (15 μl of beads volume) were added for 30 min at room temperature to immobilize the fusion protein. Beads were then washed three times with cold binding buffer supplemented with 120 mM NaCl, and the retained proteins were eluted with Tris-HCl, pH 8, 75 mM reduced glutathione and analyzed by SDS-polyacrylamide gel electrophoresis.

Wild-type and mutant 43-kDa proteins were tested for ATPase activity after incubating with [γ-^{32}P]ATP and measuring $^{32}P_i$ liberation using a charcoal adsorption assay. The method was derived from that previously described for GTPase assays (16). The ATPase activity was measured in a volume of 10 μl at 25 °C. The reaction mixture contained 10 μM cleaved 43-kDa protein in binding buffer in the presence of various concentrations of [γ-^{32}P]ATP. The amount of free $^{32}P_i$ was determined by scintillation counting. The specific novobiocin-sensitive ATPase activity was determined by including 10 μM novobiocin in the assay.

Crystallization of the Y5S Mutant 43-kDa Fragment and Data Collection—The molecule was crystallized in the presence of ADPNP and in the absence of Mg^{2+} using the sparse matrix crystallization screening kit developed by Jancarik and Kim (17) and commercialized by Hampton Research (Riverside, CA). The conditions are different from those previously described for the wild-type fragment (7). Crystals were grown at 4 °C by vapor diffusion techniques against a reservoir solution containing 100 mM Hepes, pH 7.5, 4% PEG400, 0.2 M ammonium sulfate. The hanging drops were formed by mixing 4 μl of protein (20 mg/ml), 1 μl of 10 mM ADPNP, and 5 μl of reservoir buffer. Within 3 weeks crystals formed; they belonged to the orthorhombic space group $P2_12_12$, with unit cell dimensions a = 84.7 Å, b = 137.4 Å, c = 78.9 Å and two molecules per asymmetric unit. The crystal of size of 800 × 400 × 30 μm was rapidly soaked in a cryoprotectant solution (the reservoir buffer including 25% glycerol w/v) and then flash-cooled to 120 K in an evaporating nitrogen stream. 2.3-Å resolution diffraction data were collected from a single crystal at 120 K using synchrotron radiation at LURE (Orsay, France). X-ray diffraction data were processed with the MarXDS package (18); the corresponding statistics are summarized in Table I.

TABLE I
Crystallographic data collection

X-ray source	LURE beam line W32 (Orsay)
Wavelength (Å)	0.91
Detector system	Imaging plate MarResearch
No. of crystals	1
Temperature at crystal (K)	120
Space group	$P2_1$, 2_1, 2
Cell parameters, a, b, c (Å)	84.7, 137.4, 78.9
Resolution (Å)	15.0–2.3
No. of reflections	
Observed	114,762
Unique	33,856
Redundancy	3.4
Completeness (%)	80 (56)[a]
I/s(I)	26.4 (5.5)[a]
R(I) merge	4.4

[a] For the highest resolution shell 2.5–2.3 Å.

Structure Determination—The structure was solved by molecular replacement using the program AMoRe (19) with the atomic coordinates of a single monomer of the wild-type 43-kDa N-terminal fragment of the GyrB subunit complexed to ADPNP as a model (7). The self-rotation analysis indicated a dimer axis along the y axis. The cross-rotation search was done at the resolution of 10.0–4.0 Å using the full atom model without the first 15 residues that form an arm in the wild-type structure. The first rotation peak was more than 3 times higher than the next one. It was necessary to split it artificially into 2 close peaks differing by 1° in order to allow AMoRe to find simultaneously the position of two independent monomers. The amplitude correlation for the rigid body refined model was 0.66 (crystallographic r = 0.38). The resulting dimer (Fig. 3*A*) is similar to the one reported for the wild-type molecule (7).

The refined model was obtained after several iterations of model refinement using the program X-PLOR (20) and model building steps with the program O (21). The final iterations were done including the data up to 2.3-Å resolution. The non-crystallographic symmetry between the monomers was fixed at the beginning of the refinement and removed at the end. The electron density maps were calculated with the R_{free}-based figure of merit (22, 23). The density growing technique (24) was used at different steps of structure determination and analysis in order to improve weak density in several difficult cases like the first 3 residues in the N-terminal regions. The MAPMAN suite (25) and the programs CONFOR (26), PROCHECK (27), and PROMOTIF (28) were used.

Water molecules were placed in the asymmetric unit independently for each monomer. More than half of them have a partner at the position related by the non-crystallographic symmetry operation. Three peaks of the electron density, initially interpreted as waters, were refined with small B factors (from 10 to 2 Å^2). Their density shape and the chemical contacts led to re-interpretation of these peaks as sulfate ions. Refinement statistics are given in Table II. Illustrations were done with the program SETOR (29). The coordinates of the crystal structure have been deposited in the Protein Data Bank.

RESULTS

GyrB Dimerization Is Affected by Tyr-5 and Ile-10 Point Mutations—GyrB subunit dimerization is an essential step during the catalytic DNA transfer driven by DNA-gyrase, the bacterial type II DNA topoisomerase. Crystallographic analysis of the 43-kDa nucleotide-binding domain suggested that the first 14 N-terminal residues of *E. coli* GyrB subunit form an arm that stabilizes both intersubunit contacts and ATP binding (7). We wished to provide experimental evidence that dimerization is critical for ATPase activity. Therefore, we sought to generate mutants with reduced dimerization. To accomplish

TABLE II
Refinement statistics

Model			
Residues	2 × 391		
Co-enzyme	2 × 1		
Glycerol	2 × 1		
Sulfate	3		
Water	505		
Mon2/Mon1 domain relationships			
Domain 1			
Rotation angles (Euler, °)	268.3	176.0	264.9
Translation (Å)	51.1	3.0	41.7
Domain 2			
Rotation angles (Euler, °)	253.5	177.3	251.5
Translation (Å)	50.4	2.2	41.4
Resolution (N reflections)	R (R_{free})		
2.3–7.0 Å (31,559)	18.1 (27.3)		
2.3–6.0 Å (30,657)	17.1 (27.1)		
Geometry statistics			
r.m.s.[a] Δbond	0.008 Å		
r.m.s. Δangle	1.6 °		
r.m.s. Δdihedral	25 °		
r.m.s. Δimprop	3.3 °		
Ramachandran plot zones			
Most favorable	597 (87.0%)		
Additional allowed	87 (12.6%)		
Disallowed	2 (0.4%)		

[a] r.m.s., root mean square.

this, we mutated the two most conserved residues of the N-terminal arm, Tyr-5 and Ile-10.

The non-hydrolyzable ATP imido analog ADPNP stabilizes the dimer of 43-kDa GyrB N-terminal domain (6, 30). We used GST pull-down assays to measure the interaction between GyrB 43-kDa and its Y5F, Y5S, and I10G mutant derivatives; wild-type (WT) and mutants were expressed as GST fusion proteins in *E. coli*. When GST-WT was incubated with thrombin-cleaved WT in the absence of ADPNP, only the GST-WT was retained on Sepharose beads (Fig. 1, *lane C*). By contrast, in the presence of ADPNP (Fig. 1, *lane 1*), we observed two species corresponding to GST-WT and WT, which indicates that the interaction between these two proteins is ADPNP-dependent. Moreover, no specific binding of GyrB 43-kDa to either glutathione-Sepharose beads or GST protein was observed in the presence of ADPNP. Fig. 1*A* also shows the interactions of the mutant proteins with the WT fragment. GST-WT was incubated with either Y5F (*lane 2*) or Y5S (*lane 3*) mutants in the presence of ADPNP. The interaction between GST-WT and the mutant proteins was reduced at least 5-fold as compared with GST-WT/WT. Similar results were obtained when the WT fragment was incubated with GST-Y5F and GST-Y5S mutant proteins. We also studied the homotypic interaction between Y5F or Y5S proteins (Fig. 1*A*, *lanes 4* and *5*, respectively). Interaction between Y5F or Y5S mutant proteins was approximately 20-fold reduced when compared with the WT protein (*lane 1*). The interaction of I10G mutant protein with the GST-WT protein was also tested. GST-WT was incubated with the I10G (*lane 6*) mutant in the presence of ADPNP. GST-I10G was also incubated with the cleaved mutant protein (*lanes 7*). Under these conditions, we could not detect the formation of homodimers in the presence of ADPNP; interaction of the mutants with WT protein was also dramatically affected by the I10G mutation. Table III summarizes the protein dimerization results.

Nucleotide Binding Domain Dimerization Enhances the ATPase Turnover—Dimerization of the GyrB 43-kDa N-terminal domain upon ATP binding is reversed by the hydrolysis of ATP into ADP and P_i. To test if dimerization of the nucleotide

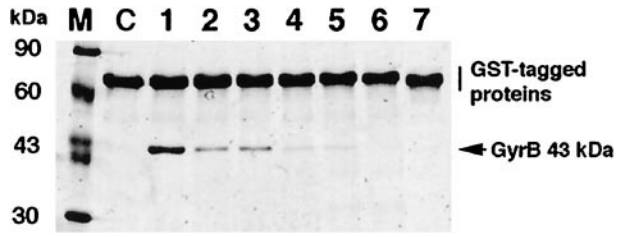

FIG. 1. **Effect of the Y5F and Y5S point mutations on the oligomerization of the 43-kDa N-terminal GyrB fragment in the presence of ADPNP.** GST fusion 43-kDa proteins (GST-tagged protein) were incubated in the presence of cleaved 43-kDa N-terminal GyrB fragments (GyrB 43-kDa) and 0.5 mM ADPNP for 12 h incubation at 25 °C. The fusion proteins were immobilized by glutathione-Sepharose beads. Following extensive washes with cold incubation buffer supplemented with 120 mM NaCl, the retained proteins were analyzed by SDS-polyacrylamide gel electrophoresis. *M*, low molecular weight markers (Amersham Pharmacia Biotech); a control experiment with GST-WT 43-kDa fusion protein and cleaved WT 43-kDa protein was done in the absence (*lane C*) or presence of ADPNP (*lane 1*). Incubation of GST-WT 43-kDa fusion protein with either Y5F- (*lane 2*) or Y5S- (*lane 3*) or I10G (*lane 6*)-cleaved mutant 43-kDa proteins were done to analyze the ability of these proteins to form mixed complexes in the presence of ADPNP. Finally, the Y5F (*lane 4*), Y5S (*lane 5*), and I10G (*lane 7*) mutant GST 43-kDa fusion proteins were incubated in the presence of ADPNP with their corresponding cleaved 43-kDa mutant fragments.

TABLE III
Summary of interactions between WT and mutant GyrB 43-kDa fragments in the presence of ADPNP

The symbols used are as follows: −, no interaction; +, weak interaction; ++, medium interaction; +++, strong interaction.

	WT	Y5F	Y5S	I10G	Δ1–14
GST-WT	(1)[a]	(2)	(3)	(6)	NS[b]
	+++	++	++	−	−
GST-Y5F	NS	(4)	NS	ND[c]	ND
	++	+	+		
GST-Y5S	NS	NS	(5)	ND	ND
	++	+	+		
GST-I10G	NS	ND	ND	(7)	ND
	−			−	
GST-Δ1–14	NS	ND	ND	ND	NS
	−				−

[a] Parentheses represent the lane number in Fig. 1*A*.
[b] NS, not shown.
[c] ND, not determined.

binding domain was required for ATPase activity, each of the Y5F, Y5S, I10G and Δ1–14 GyrB 43-kDa mutants was tested for their ability to bind and hydrolyze [γ-^{32}P]ATP. The kinetics of novobiocin-sensitive ATP-hydrolysis activity for each enzyme were obtained at a protein concentration of 10 μM (Fig. 2*A*). Novobiocin belongs to the family of coumarin antibiotics that compete with ATP at its binding site on DNA-gyrase B subunit. As expected, preincubation of WT 43-kDa protein for 1 h with 10 μM novobiocin completely inhibited the ATPase activity. Fig. 2*A* shows the WT 43-kDa ATPase activity in the presence of 0.5 mM ATP. The ATP hydrolysis catalyzed by the WT 43-kDa increased linearly during the first 60 min, and a plateau due to accumulation of ADP by-product was reached within 120 min at 25 °C. Under similar conditions, Y5F and Y5S 43-kDa proteins also showed a novobiocin-sensitive ATPase activity. By contrast to the WT protein, the ATP hydrolysis catalyzed by Y5F and Y5S mutants was observed only after a lag of 30 min, probably reflecting the conversion between two protein conformations with low and high affinity; the rates of ATP hydrolysis were decreased 3- and 5-fold, respectively. We also measured the novobiocin-sensitive ATP hydrolysis of the I10G mutant 43-kDa protein. By contrast to the Y5F and Y5S mutants, the ATP-hydrolysis activity was significantly decreased, and no lag was observed at the first

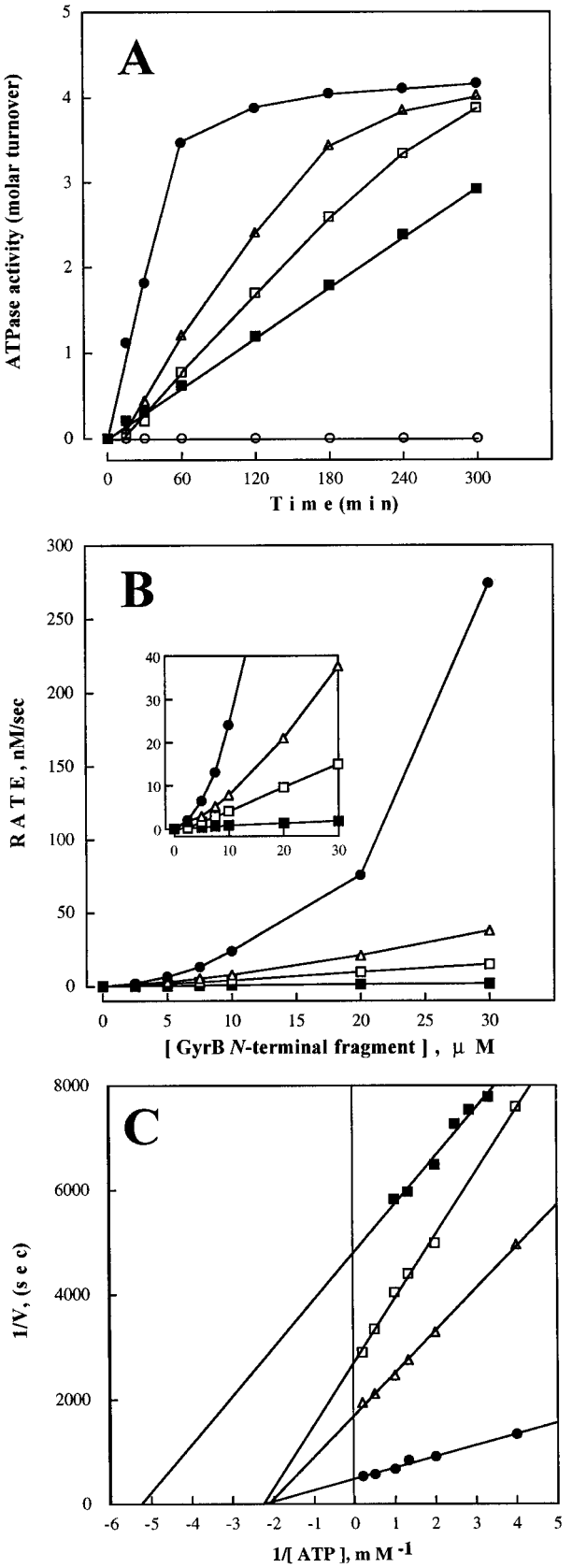

FIG. 2. **Kinetic analysis of the ATPase activity of WT 43-kDa GyrB fragment and of fragments containing Y5F and Y5S mutations and Δ1–14 deletion.** The free $^{32}P_i$ released after ATP hydrolysis was determined as described under "Experimental Procedures." *A*, effect of the Tyr-5 and Ile-10 point mutations and N-terminal arm deletion on the kinetic of ATP hydrolysis. Protein concentration was 10 μM; ATP concentration was 500 μM. *y* axis is expressed as mole of ATP hydrolyzed per mol of 43-kDa protein (molar turnover). *B*, ATPase activity of the 43-kDa mutant proteins as a function of protein concentration. Rates are initial velocities. ATP concentration was 1 mM. GyrB N-terminal fragment corresponds to the 43-kDa protein. *C*, at constant enzyme concentration (10 μM), the turnover rates for ATP hydrolysis by WT, Y5F, and Y5S 43-kDa GyrB fragments were measured in the presence of varying concentrations of ATP. WT (●); Y5F (△); Y5S (□); I10G (■); Δ1–14 (○).

time of the kinetic. The Δ1–14 deletion mutant 43-kDa protein did not show any ATP-hydrolysis activity.

As shown in Fig. 2*B*, the ATPase activity of WT 43-kDa protein is not linearly dependent upon enzyme concentration over the range 2.5–30 μM, in agreement with previous biochemical characterization (6). This greater than first-order dependence of ATPase activity on enzyme concentration demonstrates that the 43-kDa protein does not follow Michaelis-Menten kinetics and indicates that the active form of the protein may be an oligomer. Similar experiments were performed with the dimerization-deficient 43-kDa mutant proteins in order to determine the effect of Tyr-5 and Ile-10 point mutations on the allostery of the ATPase. As for the WT, the ATPase activities of Y5F and Y5S 43-kDa mutants were not found to be linearly dependent upon enzyme concentration (Fig. 2*B*, *inset*). However, the cooperativity of these mutant ATPases is significantly affected by comparison to the WT ATPase activity that is strongly enhanced at concentrations above 10 μM enzyme concentration, consistent with the partial defect in enzyme dimerization detected by GST pull down (Figs. 1 and 2*B*). By contrast, the I10G mutant 43-kDa protein, which does not dimerize, exhibits a low ATPase activity that presents an apparent first-order dependence on enzyme concentration over the range 2.5–30 μM. These results demonstrate that the effect of mutations in the Tyr-5 and Ile-10 residues on ATPase activity is due to an effect on dimerization.

To characterize further the effect of the Y5F, Y5S, and I10G point mutations on the ATPase activity of the 43-kDa protein, ATPase apparent constants were determined. The reaction was modeled as a pseudo-first order process since the 43-kDa fragment demonstrates the familiar hyperbolic dependence of rate on substrate ATP concentration at constant enzyme concentration (6). The apparent K_m and k_{cat} values determined at a 10 μM fragment concentration were calculated from a double-reciprocal plot of the novobiocin-sensitive ATPase rates *versus* ATP concentrations (Fig. 2*C*). The apparent turnover value $k_{cat(app)}$ for the WT 43-kDa protein was 20×10^{-4} s^{-1}. Lower values, $\sim 6 \times 10^{-4}$, $\sim 4 \times 10^{-4}$, and $\sim 2 \times 10^{-4}$ s^{-1} were calculated for the Y5F, Y5S, and I10G mutants, respectively. The $K_{m(app)}$ value for ATP hydrolysis of the 43-kDa fragment, ~0.45 mM, was not affected by the Y5F and Y5S point mutations. The I10G mutant 43-kDa protein had a lower $K_{m(app)}$ value, ~0.2 mM. These results indicate that the Tyr-5 and Ile-10 residues are not significantly involved in the binding of their natural substrate ATP and that dimerization of GyrB 43-kDa domain enhances about 10-fold the turnover rate for ATP hydrolysis at a 10 μM enzyme concentration.

Crystal Structure of the Y5S Mutant, the Dimeric Interface—The previous crystallographic analysis of *E. coli* GyrB 43-kDa WT fragment implicated a conserved tyrosine residue at position 5 in both intersubunit contacts and ATP-binding site formation (7). However, the structural requirement of this residue for both GyrB dimerization and activity was unknown. To analyze in detail the dimeric interface and its requirement for the formation of the catalytic site, we solved the structure of the Y5S mutant at 2.3-Å resolution. The Y5S mutant protein forms a dimer (Fig. 3*A*). Each monomer contains two distinct domains, an N-terminal one of 24 kDa (domain 1, aa 2–220)

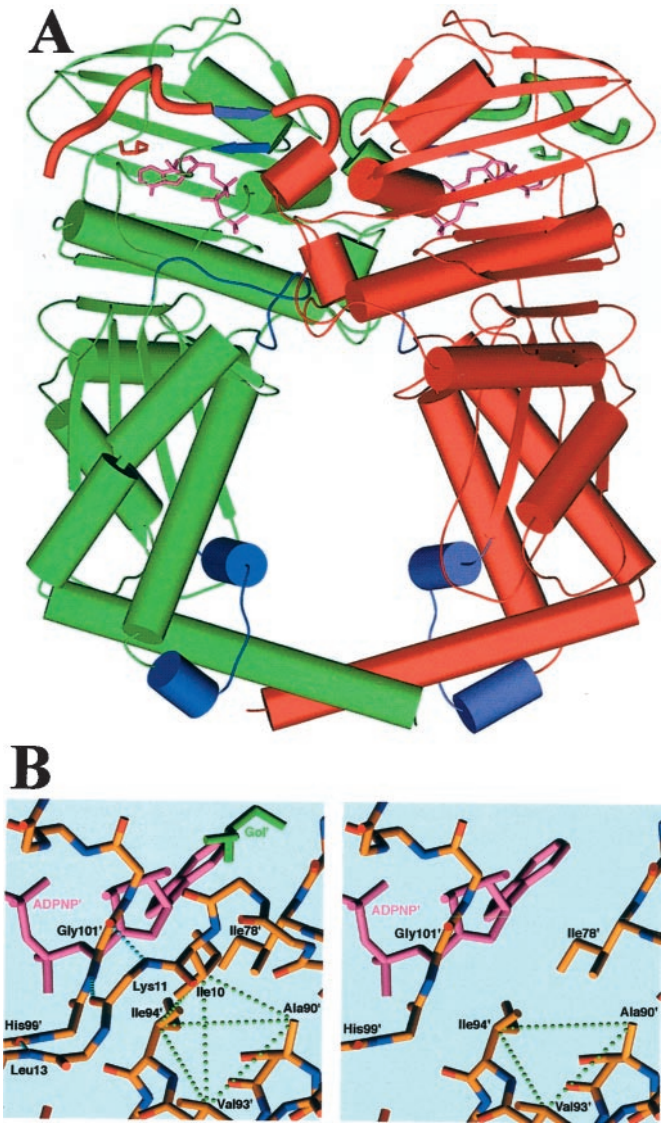

FIG. 3. **Structure of the Y5S mutant GyrB 43-kDa N-terminal fragment complexed with ADPNP.** *A*, general view of the mutant structure. Glycerol molecules are shown in *red* and *green*. The ADPNP molecules are shown in *magenta*. New helical parts of the loops 299–315 (at the *bottom*), loops 329–340 (at the *middle*) of the second domains touching the ADPNP molecules, and the residues 11–13 and 99–101 (at the *top*), making hydrophilic contacts, are shown in *violet* and *blue*, respectively. The N-terminal arms are shown as *ribbons,* and other loops are shown as *ropes*. Note a slight difference in the conformation of the first residues of the N-terminal arms. *B*, interactions of the N-terminal arm. *Left panel*, the hydrophilic interactions of the main chain atoms of the Lys-11 and Leu-13 with the main chain atoms of the second monomer are shown by *light-blue balls*. The *green balls* show the tetrahedron formed by the C-β atoms of Ile-10 of the first monomer and the Ala-90′, Val-93′, and Ile-94′ residues of the second monomer (indicated by a prime after the residue number). *Right panel*, view where the N-terminal arm is omitted in the dimer interface.

and a C-terminal one of 19 kDa (domain 2, 221–392). Except for a modification of the WT long loop between residues 298 and 315 where the electron density maps showed clearly two short α-helical turns (302–306 and 312–315) surrounding the long C-terminal helix (Fig. 3*A*), the overall fold of each domain is similar to that observed in the WT structure.

Most of the dimer contacts are through the N-terminal arm (residues 2–16) and the following helix (residues Lys-21, Arg-22, Met-25, Tyr-26, and Gly-28). Amino acids forming the arm protrude from one monomer to wrap around the 24-kDa domain 1 of the other subunit. The dimer interface is not strongly affected by the Y5S point mutation. The electron density shows a slight shift of 0.5–1.5 Å for residues 5–10 of both mutant monomers from their WT position. Whereas the main chain of Ser-5 remains hydrogen bonded to Arg-136 as in WT structure, its side chain is too far away to interact with the bound nucleotide. A strong residual density of an extended shape can be observed in both monomers at the place of the corresponding Tyr-5 side chain in the WT model. That density could be interpreted as a glycerol molecule that has diffused in the crystal before cryocooling for data collection.

Interestingly, an entire wall of the nucleotide-binding site is stabilized by dimer contacts. This involved loop 80–90 and loop 99–117 that contains the P-loop motif G*X*X*X*G*X*G implicated in mononucleotide binding and hydrolysis site (31). Loop 80–90 and loop 99–117 do not interact but form a channel in which the invading N-terminal arm fits, making several contacts (Fig. 4). Loop 80–90 is only stabilized by the N-terminal arm of the adjacent subunit. The van der Waals contacts mediated by Val-12 and Ile-10 provide the most significant molecular interactions, which anchor the loop to the N-terminal arm. Ile-10 also forms strong hydrophobic interactions with amino acids located in the two rigid helices adjacent to the loop. The C-β atoms of Ile-10 side chain from one monomer and those of Ala-90′, Val-93′, Ile-94′ from another monomer form an almost ideal hydrophobic tetrahedron of 7 Å edge (Fig. 3*B*).

Loop 99–117 that forms a lid over the ATP-binding site is maintained in its position by both hydrophilic and hydrophobic interactions through the short β-sheet formed by residues 11–13 (Fig. 4). The main chains of residues Lys-11 and Leu-13 of one monomer form hydrogen bonds with those of residues Gly-101′ and His-99′ of the second monomer, respectively. These interactions are further stabilized by van der Waals contacts between the C-γ atom of Leu-13 and the aromatic cycle of Phe-104′ and between the C-β atoms of Val-12 and Val-97′, Ala-100′. As a result, an alternation of hydrophilic and hydrophobic clusters contributes to positioning and stabilizing the loop 80–90/arm/loop 99–117 complex forming a 3-layer sandwich in front of the bound nucleotide (Fig. 4*C*). Interestingly, Leu-98 and Val-118 residues forming the roots of loop 99–117 are part of an extensive network of hydrophobic contacts that structure the heart of the ATP-binding domain independently of other contacts brought by the dimerization process. Thus, one important part of loop 99–117 and the entire loop 80–90 are only stabilized in their observed positions by dimeric contacts induced upon nucleotide binding, indicating that the folding of the secondary structural elements of the ATP-binding pocket is strongly dependent of the presence of ATP and also of the monomeric or dimeric state of the enzyme.

The ATP-binding Site—The ADPNP molecule binds in a cavity formed by the antiparallel β-sheet and three α-helices of domain 1. It is covered by the long flexible loop 99–117 that hides the bound nucleotide and blocks its exit from the enzyme (Fig. 4*C*). Residues (100–103, 109, and 115–119) interact with the nucleotide molecule. Residues 111–118 interact also with loop 326–338 of domain 2 which itself is in contact with the γ-phosphate through Gln-335 and Lys-337 (Fig. 4, *A* and *B*). The flexible loops form an interdigitated wall.

The structure reveals the existence of a channel leading to the γ-phosphate of the ADPNP (Fig. 5). Residues 31–48, 185–196, and 272–277 as well as residues 26–28 and 335–337 line it. These loops are stabilized by intermolecular contacts with their 2-fold symmetry-related loops. Ions or solvent molecules can reach the bound ATP through this tunnel. Its diameter is also sufficient to let an orthophosphate group leave the gyrase dimer after hydrolysis. In both monomers, the tunnel is filled by a chain of ordered solvent molecules, one of them being in

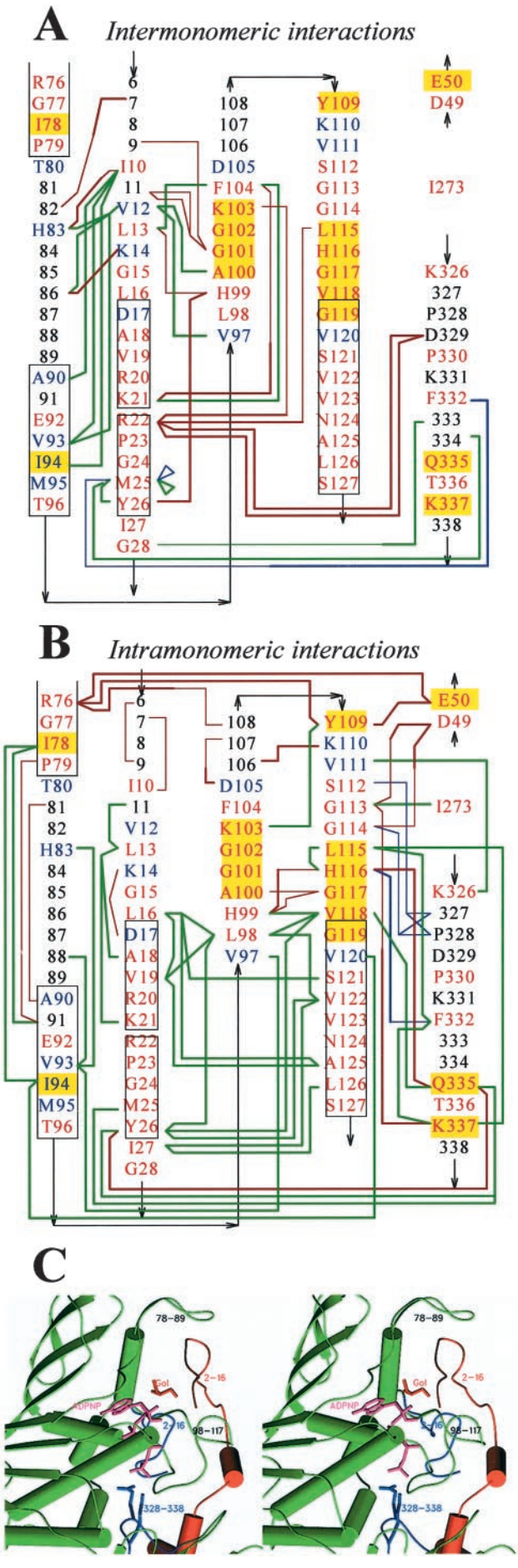

contact with O-γ1 of the ATP (Fig. 5). This molecule, noted S1, is positioned by H bonds with the O-ϵ2 atom of Glu-42 and the main chain carbonyl oxygen of Gln-335 and could play a critical role in the catalytic process.

Glu-42 and Gln-335 are ideally located to act as general bases and activate the S1 water molecule for nucleophilic attack on the γ-phosphate. In our structure, the magnesium ion is absent. Superposition of this structure to that of the wild-type fragment containing the cation reveals that its presence slightly changes the orientation of the β- and γ-phosphates favoring the interaction between the water molecule S1 and the hydrogen acceptor Glu-42 rather than with Gln-335 (Fig. 6). Thus in the presence of magnesium only, Glu-42 could efficiently activate the solvent molecule S1 for a nucleophilic substitution reaction by polarization via hydrogen bonding, consistent with the model for a trans-esterification reaction mediated by a water molecule previously proposed by Jackson and Maxwell (34).

DISCUSSION

Electron microscopy studies on purified topoisomerase II enzymes have shown that the human and yeast N-terminal domains, homolog to the GyrB 43-kDa domain, are flexible and can move freely in the absence of nucleotide (11, 32). Upon ADPNP binding, they adopt a closed dimeric conformation similar to that observed in the conformation of *E. coli* GyrB 43-kDa complexed to ADPNP (7). This dimer allows the capture of a DNA duplex that is translocated during topoisomerization reaction (9). Interestingly, it is also associated to the enzyme turnover via activation of the hydrolysis of the bound ATP.

Previous biochemical and structural studies have defined a functional model for GyrB ATPase activity (6, 7). Upon the initial binding of one ATP molecule to a free subunit, the primary GyrB monomer-ATP complex dimerizes and becomes highly efficient for hydrolyzing ATP (6). The rate-limiting step of the ATPase reaction is the dimerization step. However, a key untested prediction of this model is that dimerization is critical for ATPase activity. To provide experimental evidence, we searched for dimerization-deficient mutant proteins in order to study their ATPase activity.

The crystal structure of GyrB 43-kDa domain bound to ADPNP displays a frozen conformation of the nucleotide-binding site in its stable dimeric form. Analysis of conserved residues lining the nucleotide-binding site reveals a peculiar role for the Tyr-5 side chain that binds to the 2′-hydroxyl group of the ADPNP ribose in the adjacent subunit, suggesting that this conserved residue plays a critical role in GyrB dimerization

Fig. 4. **Principal interactions between flexible model parts at the ATP-binding region.** *A*, intermonomeric interactions. Interaction of the N-terminal arm and the loops 80–90, 97–118, and 330–337 are shown. *Boxes* indicate α-helices. Conserved residues are shown in *blue* with their names, and very highly conserved residues are in *red*. Residues interacting with the ADPNP molecule are marked by *yellow rectangles* (A100 interacts through a water molecule). The water-mediated interactions are shown in *blue*, and hydrophilic ones are shown in *ochre* and hydrophobic contacts in *green*. *Thick lines* correspond to side chain interaction, and the *thin one* to main chain interactions. Residues 6–28 arise from the opposite subunit in the dimer. Note, in particular, the numerous hydrophobic interactions of the N-terminal arm with the residues of the other monomer, the importance of Leu-98 for the intramonomeric interactions, and the role of Met-25 and Tyr-26 for both inter- and intramonomeric interactions. *B*, intramonomeric interactions. *C*, stereoscopic view showing the interdigitation of flexible loops at the ATP-binding pocket. In the monomer 1, secondary structural elements of domain 1 (aa 2–220) are shown in *green* except for the loop 326–338 which is indicated and colored in *blue*. The loops 80–90 and 99–117 are also indicated. The N-terminal arm (aa 2–16) and following helices of the adjacent monomer in the dimer are shown in *red* like the glycerol molecule (*Gol*). ADPNP is shown in *magenta*.

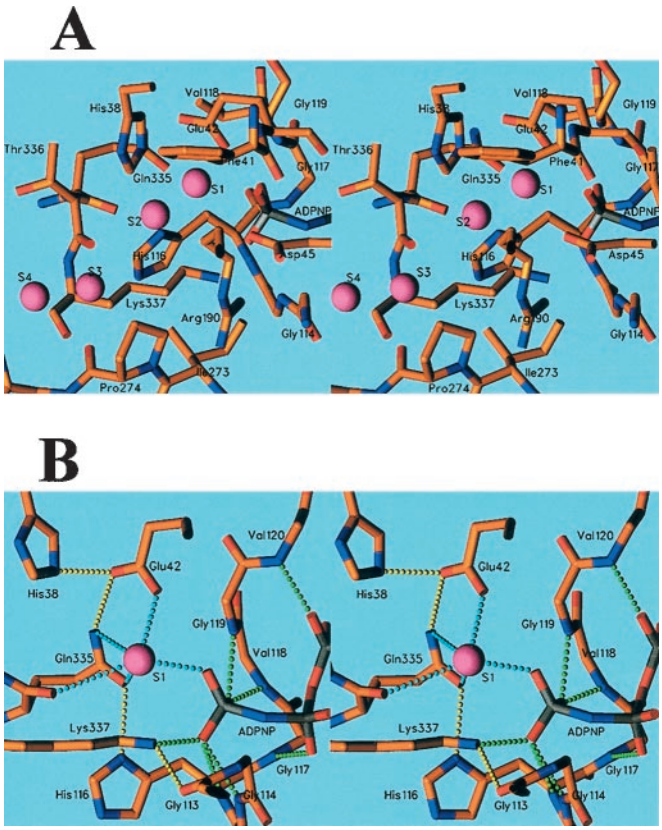

FIG. 5. **The tunnel in a gyrase monomer at the phosphate end of the ADPNP.** *A*, side chains of amino acids making front "walls" of the tunnel are indicated. All shown solvent molecules, indicated by balls in *magenta* (S1 to S4), have temperature factor varied from 15 to 32 Å^2. *B*, interactions with the solvent molecule S1 located near the γ-phosphate group. Note the interactions of the main chain nitrogens of the sequence 114–120 with the ADPNP molecule fixing the orientation and neutralizing charge of the three phosphate groups. S1 indicates the potential reactive water molecule interacting with O-γ1 of the ADPNP (2.6 Å distance), with O-ϵ2 of Glu-42 (2.8 Å), with N-ϵ2 of Gln-335 (3.1 Å), with O-ϵ1 of Gln-335 (2.6 Å), and with O of Gln-335 (3.4 Å). Note also close contacts between O-ϵ1 of Glu-42 and N-ϵ2 of His-38 (2.9 Å), O-ϵ1 of Gln-335, and N-δ1 of His-116 (2.9 Å), between N-ζ of Lys-337 and O of Gly-113 (2.8 Å), between N-ζ of Lys-337 and O-γ2 of ADPNP (2.7 Å), between N-ϵ2 of Gln-335 and O of Tyr-26 (2.8 Å), between N-ϵ2 of Gln-335 and O-ϵ1 of Glu-42 (3.2 Å). Contacts are shown by *small balls* in *yellow, light blue,* and *green.*

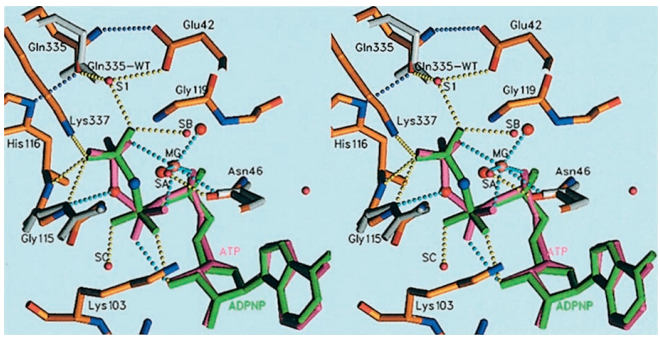

FIG. 6. **Conformational changes near the Mg^{2+}-binding site.** ATP/ADPNP, protein conformations, and main interactions are shown near the Mg^{2+}-binding site. ATP is shown in *magenta* and ADPNP in *green* (O and N atoms are indicated in *red* and *blue balls*, respectively). Protein is shown for the Y5S mutant fragment; Asn-47 and Gln-335 side chains and Leu-115 main chain of the wild-type protein are shown in *gray*. In the wild-type complex, Mg^{2+} (*big orange ball*) interacts with O-α2, O-β1, and O-γ1 of the phosphate groups, Asn-46 O-γ1 and two water molecules (*big red balls*). O-β2 interacts with the sugar and O-β3 interacts with Leu-115 main chain NH group. *Small light blue balls* represent all interactions. In the case of the Y5S mutant fragment complexed with salt-free ADPNP, the orientation of the β-γ phosphates is completely different. The place of Mg^{2+} is empty, but there are two water molecules (*small magenta balls* indicated as SA and SB) at positions very close to the original Mg^{2+}-bound water molecules; one of them interacts with O-γ1, and the second interacts with Asn-46 O-δ1. O-β1 interacts now with the sugar and O-β2 with a new water molecule, SC. After slight rearrangement of Leu-115, its main chain NH group interacts only with O-γ1. *Small yellow balls* indicate all interactions. S1 is the first solvent molecule in the water channel leading to the protein surface. Note the significant change in the Gln-335 conformation. Interaction of the adenine base and surrounding water molecules are not shown.

and function (7). We recently showed that phenylalanine and serine substitutions of Tyr-5 severely affect all ATP-dependent reactions catalyzed by DNA-gyrase on DNA, *e.g.* supercoiling and decatenation of circular DNA molecules (13, 33). Furthermore, DNA binding did not stimulate the ATPase activity of these mutants. We therefore proposed that Tyr-5 is a crucial residue for GyrB dimerization and thus for DNA transfer during catalytic transfer of DNA duplex catalyzed by gyrase.

In the present study, we show that Y5F or Y5S point mutations affect dimer interactions (Fig. 1*A*). However, the formation of mutant-WT heterodimers indicates that Tyr-5 plays a role but is not essential at the dimer interface. This is further confirmed by the crystal structure of the Y5S mutant complexed with ADPNP. As shown in Fig. 3*A*, the overall three-dimensional structure of the mutant monomer is similar to that previously described for the WT protein (7). Only minor conformational differences were observed for residues 2–9. At the site normally occupied by the Tyr-5 phenolic group in the WT structure, an extra density interpreted as a bound glycerol was found. In normal physiological conditions, three water molecules that would fill the cavity while maintaining the stabilizing H bond network could easily replace this new cofactor. This finding is in agreement with our observation that the turnover of the ATPase activity of the Y5S and Y5F GyrB mutants is reduced but not inhibited (Fig. 2), (33).

To determine the relative importance of dimerization in the activation of ATP hydrolysis, we looked for mutants unable to dimerize. Upon analysis of the three-dimensional structure, we identified two residues (Ile-10 and Val-12) of the N-terminal arm that form numerous hydrophobic contacts with the adjacent subunit and could be crucial for dimerization (Figs. 3*B* and 4). We then chose Ile-10 as the mutagenesis target because, in contrast to Val-12, it does not interact with the flexible loop 99–117 that participates to the nucleotide-binding site. Instead, Ile-10 side chain anchors the invading N-terminal arm through the formation of a strong hydrophobic cluster at the dimer interface (Fig. 3*B*). As shown in Figs. 1 and 2, Gly mutation of the Ile-10 residue severely affected the ability of the ATPase domain to dimerize without altering the affinity for ATP. Interestingly, the ATPase turnover was severely decreased (10-fold at 10 μM enzyme concentration) but not completely inhibited, and the cooperativity of the ATPase reaction was lost. These results provide evidence that the 43-kDa domain monomer is still able to hydrolyze ATP, but the dimerization process observed with the wild type is essential for the cooperativity of the ATPase reaction.

To understand the structural requirement of GyrB dimerization for ATPase activity, we analyzed the nature of intra- and intermonomeric contacts (Fig. 4). The bound nucleotide recruits several amino acids of loops 99–117 and 326–338. Within the dimer structure, these loops form an extensive network of intermolecular van der Waals contacts and direct or water-mediated hydrogen bonds. The additional interactions brought by dimerization stabilize the potentially flexible loops of the binding pocket (residues 80–90, 99–117, and 326–338), which are contacted by the N-terminal arm and adjacent helices (aa 2–28) of the dimeric partner. These dimeric contacts

most probably affect the P-loop signature motif ^{114}G*XX*G*X*G located at the C terminus of the loop 99–117 (31), facilitating the orientation of the γ-phosphate in the catalytic site. More interestingly, additional dimer contacts mediated by Arg-22, Met-25, Tyr-26, and Gly-28 help to position residues 26–28 and loop 326–338 which form the walls of a little channel leading to the γ-phosphate group where solvent molecules including the reactive water molecule (S1) transit to reach the catalytic site of ATP hydrolysis (Fig. 5). Therefore, dimerization of GyrB subunits provides a unique structural mechanism to allow water molecules to activate efficiently the hydrolysis of bound ATP molecules. Upon the nucleophilic attack mediated by Glu-42 and S1 on the γ-phosphate group of the ATP molecule (Fig. 6), this little channel formed at the dimer interface may also provide an exit for the P_i liberated during ATP hydrolysis. These observations highlight a new aspect of the structure-function relationship in topoisomerase II ATPase. They provide a better understanding of the mode of action of drugs targeting the N-terminal dimer interface, for example antibiotics belonging to coumarin and cyclothialidin families.

Acknowledgments—We are grateful to A. Maxwell and D. B. Wigley for supplying the coordinates of *E. coli* 43-kDa GyrB wild-type fragment. We also thank M. Klich and P. Mauvais for advice and comments and A. M. Edwards for critical reading of the manuscript; A. Staub and collaborators for oligonucleotide synthesis and purification; S. Vicaire for DNA sequencing; L. Hoermann, C. Dupuis-Hamelin, and A. Forster for technical assistance; B. Boulay for photographic work; and L. Moulinier for assistance in preparing the illustrations.

REFERENCES

1. Gellert, M., Mizuuchi, K., O'Dea, M. H., and Nash, H. A. (1976) *Proc. Natl. Acad. Sci. U. S. A.* **73,** 3872–3876
2. Kreuser, K. N., and Cozzarelli, N. R. (1980) *Cell* **20,** 245–254
3. Menzel, R., and Gellert, M. (1994) *Adv. Pharmacol.* **29A,** 201–225
4. Maxwell, A., and Gellert, M. (1986) *Adv. Protein Chem.* **38,** 69–107
5. Reece, R. J., and Maxwell, A. (1991) *Crit. Rev. Biochem. Mol. Biol.* **26,** 335–375
6. Ali, J. A., Jackson, A. P., Howells, A. J., and Maxwell, A. (1993) *Biochemistry* **32,** 2717–2724
7. Wigley, D. B., Davies, G. J., Dodson, E. J., Maxwell, A., and Dodson, G. (1991) *Nature* **351,** 624–629
8. Roca, J., Berger, J. M., Harrison, S. C., and Wang, J. C. (1996) *Proc. Natl. Acad. Sci. U. S. A.* **93,** 4057–4062
9. Berger, J. M., Gamblin, S. J., Harrison, S. C., and Wang, J. C. (1996) *Nature* **379,** 225–232
10. Roca, J., and Wang. J. C. (1994) *Cell* **77,** 609–616
11. Schultz, P., Olland, S., Oudet, P., and Hancock, R. (1996) *Proc. Natl. Acad. Sci. U. S. A.* **93,** 5936–5940
12. Sugino, A., Higgins, N. P., Brown, P. O., Peebles, C. L., and Cozzarelli, N. R. (1978) *Proc. Natl. Acad. Sci. U. S. A.* **75,** 4838–4842
13. Brino, L., Mousli, M., Oudet, P., and Weiss, E. (1997) *Plasmid* **38,** 188–201
14. Staudenbauer, W. L., and Orr, E. (1981) *Nucleic Acids Res.* **9,** 3589–3603
15. Kaelin, W. G., Jr., Pallas, D. C., DeCaprio, J. A., Kaye, F. J., and Livingston, D. M. (1991) *Cell* **64,** 521–532
16. Mousli, M., Bronner, C., Landry, Y., Bockaert, J., and Rouot, B. (1990) *FEBS Lett.* **259,** 260–262
17. Jankaric, J., and Kim, S. (1991) *J. Appl. Crystallogr.* **24,** 409–411
18. Kabsch, W. (1988) *J. Appl. Crystallogr.* **21,** 916–924
19. Navaza, J. (1994) *Acta Crystallogr. Sec. A* **50,** 157–163
20. Brünger, A. T. (1992) *X-Plor, A System for X-ray Crystallography and NMR,* Version 3.1, Yale University Press, New Haven, CT
21. Jones, T. A., Zou, J. Y., Cowan, S. W., and Kjeldgard, M. O. (1991) *Acta Crystallogr. Sec. A* **47,** 110–119
22. Lunin, V. Y., and Skovoroda, T. P. (1995) *Acta Crystallogr. Sec. A* **51,** 880–887
23. Urzhumtsev, A. G., Skovoroda, T. P., and Lunin, V. Y. (1996) *J. Appl. Crystallogr.* **29,** 741–744
24. Urzhumtsev, A. G. (1997) *Acta Crystallogr. Sec. D* **53,** 540–543
25. Kleywegt, G. J., and Jones, T. A. (1996) *Acta Crystallogr. Sec. D* **52,** 826–828
26. Urzhumtseva, L. M., and Urzhumtsev, A. G. (1996) *CCP4 Newsl. Protein Crystallogr.* **32B,** 41–43
27. Laskowski, R. A., MacArthur, M. W., Moss, D. S., and Thornton, J. M. (1991) *J. Appl. Crystallogr.* **26,** 283–291
28. Hutchinson, E. G., and Thornton, J. M. (1996) *Protein Sci.* **5,** 212–220
29. Evans, S. V. (1993) *J. Mol. Graph.* **11,** 134–138
30. Ali, J. A., Orphanides, G., and Maxwell, A. (1995) *Biochemistry* **34,** 9801–9808
31. Bossemeyer, D. (1994) *Trends Biochem. Sci.* **19,** 201–205
32. Benedetti, P., Silvestri, A., Fiorani, P., and Wang, J. C. (1997) *J. Biol. Chem.* **272,** 12132–12137
33. Brino, L., Bronner, C., Oudet, P., and Mousli, M. (1999) *Biochimie* (*Paris*) **81,** 973–980
34. Jackson, A. P., and Maxwell, A. (1993) *Proc. Natl. Acad. Sci. U. S. A.* **90,** 11232–11236
35. Deleted in proof
36. Deleted in proof